

# Dynamic instabilities and turbulence of merged rotating Bose-Einstein condensates

Anirudh Sivakumar,<sup>1</sup> Pankaj Kumar Mishra,<sup>2</sup> Ahmad A. Hujeirat,<sup>3</sup> and Paulsamy Muruganandam<sup>1</sup>

<sup>1</sup>*Department of Physics, Bharathidasan University, Tiruchirappalli 620 024, Tamil Nadu, India*

<sup>2</sup>*Department of Physics, Indian Institute of Technology Guwahati, Guwahati 781039, Assam, India*

<sup>3</sup>*Interdisciplinary Center for Scientific Computing,  
The University of Heidelberg, 69120 Heidelberg, Germany*

(Dated: February 29, 2024)

We present the simulation results of merging harmonically confined rotating Bose-Einstein condensates in two dimensions. Merging of the condensate is triggered by positioning the rotation axis at the trap minima and moving both condensates towards each other while slowly ramping their rotation frequency. We analyze the dynamics of the merged condensate by letting them evolve under a single harmonic trap. We systematically investigate the formation of solitonic and vortex structures in the final, unified condensate, considering both non-rotating and rotating initial states. In both cases, merging leads to the formation of solitons that decay into vortex pairs through snake instability and subsequently, these pairs annihilate. Soliton formation and decay-induced phase excitations generate sound waves, more pronounced when the merging time is short. We witness no sound wave generation at sufficiently longer merging times that finally leads to the condensate reaching its ground state. With rotation, we notice off-axis merging (where the rotation axes are not aligned), leading to the distortion and weakening of soliton formation. The incompressible kinetic energy spectrum exhibits a Kolmogorov-like cascade [ $E(k) \sim k^{-5/3}$ ] in the initial stage for merging condensates rotating above a critical frequency and a Vinen-like cascade [ $E(k) \sim k^{-1}$ ] at a later time for all cases. Our findings hold potential significance for atomic interferometry, continuous atomic lasers, and cosmic events related to the remnants of binary neutron-star mergers.

## I. INTRODUCTION

Mergers of Bose-Einstein condensates (BECs) have been the topic of great interest among the ultracold community owing to their wide applications in building up many futuristic tools such as matter-wave interferometry, continuous atom lasers, atomtronics, etc. [1–3]. Experimentally condensate mergers have been realized in the laboratory and further investigated extensively by Scherer and group [4], who demonstrated a systematic formation of the vortices as a result of the controlled merging between the condensates. This observation played a pivotal role in establishing a one-to-one relation between the dynamical instability of merged condensate along with the appearance of topological defects formed via phase transitions, popularly termed the Kibble-Zurek mechanism [5, 6]. To this end, another successful experiment on the condensate merger was carried out by Chikkatur [7] using optical tweezers, who observed the evaporative loss of atoms in the final state of the condensate and further systematically demonstrated that the randomized initial phases could replenish BECs which further assist in developing the vortex structures in the merged state. Condensate mergers are not restricted to laboratory experiments only; it has been the essential tool in explaining the structure and dynamics of remnants of binary neutron-star merger event GW170817 [8, 9]. For instance, there are some works [10, 11] that suggest that the merger of binary stars that are mainly made of incompressible gluon-quark superfluid cores include several time scales, such as low-energy slow fusion of the core and the fast merger of surrounding envelopes of compressible and dissipative normal matter, which are

responsible for the observation of pulsars.

Several works highlight the formation of interference patterns and their properties resulting from the mergers [1, 2, 4, 12–15]. The study of the merging process and the subsequent formation of interference patterns and solitary waves has been extended to the realms of self-gravitating BECs where fundamental solitons not only form in these head-on collisions but also survive and retain their original shapes [16, 17]. Further studies on collisions of self-gravitating BECs include Paredes' observation of destructive interference patterns in solitonic collisions [18] and Schwabe's studies on gravitational cooling and density oscillations in merging of solitonic cores [19]. Recently, Nikolaieva *et al.* [20] investigated the stability of colliding vortex solitons in self-gravitating BECs for different angular momentum orientations. Similar to previous literature, they also reported the survival of solitons after head-on collisions. Self-gravitating BECs are shown to be excellent candidates for modelling rotating neutron-star interiors and their merging events [9, 21].

The merger between the condensates and the follow-up dynamical state of the merged condensate depends very much on the phases between the condensates before merging. For instance, Stickney and their colleagues [22] demonstrated that the mergers of condensates with opposite phases exhibit excited modes in the merged condensate, leading to the generation of unstable modes. The follow-up works by Mebrahtu [23] and Yi [24] suggested the phase-sensitive excitations and the influence of initial phase differences. Xiong *et al.* [12] analyzed the effect of the relative initial phase difference on the merging dynamics. Carretero-Gonzalez [25] investigated the role of recombination times on the overall structure and dynam-

ics of the merged condensate. Buchmann *et al.* [26] numerically extended the experimental study of [4] and also explored the effects of recombination/ramping time on vortex formation in a merged condensate for a given initial relative phase and conclusively demonstrated a possibility of the formation of vortex cores during mergers that very much depends on the choice of phase difference between the condensates. Scott *et al.* [27] reported the formation of persistent dark solitary waves from interference patterns, which in turn were formed from counter-propagating BEC clouds. These works, however, exclude the role of phase excitations and phase differences in the soliton dynamics. Jo *et al.* [3] reported the appearance of condensate heating and its influence on atomic numbers using external potential gradients. Apart from this, the dynamics of BECs confined in double-well potentials that exhibit a variety of complex phases have been systematically analyzed [28–30]. In recent years, the self-bound state, mainly the quantum droplet, has been considered as a prototype model to investigate the different sorts of instabilities arising due to the elastic and inelastic collision between the solitons [31, 32].

Subsequently, in the recent past, there have been several experimental and numerical investigations that focused on the role of dynamical instabilities manifest in the system as a result of merging, which eventually takes the system to a turbulent state. For instance, Kanai *et al.* [33–35] considered co-axial mergers of rotating BECs with non-uniform initial phases, where they observed the formation of spiral dark-solitons in both 2D and 3D cases, which facilitated the transfer of angular momentum between condensates. This angular momentum transfer is proportional to the initial angular momentum density difference. Furthermore, they also confirmed the formation of vortices by the decay of solitons via snake instability.

During the past few decades, research on turbulence in 2D condensates has been extensive, encompassing both decaying and forced turbulence [36–39]. Recently, rotational quantum turbulence has attracted significant interest due to its fascinating properties, contrasting with its non-rotating counterpart [40, 41]. While previous studies have identified dynamical instability in merged Bose-Einstein condensates (BECs), suggesting a potential connection to turbulence, a detailed characterization of turbulence generated through mergers is still lacking. Therefore, further investigation is necessary to understand how the recombination/merging time scales influence the generation of phase excitations and their manifestation as compressible sound waves. Additionally, prior analyses of rotational mergers typically focus on condensates merging and rotating around the same axis. Although Nikolaieva [20] explored mergers in self-gravitating rotating BECs with different angular momentum orientations, the effect of the rotation has not been considered.

In this work, we consider spatially separated, harmonically confined condensates initialized with random phases and rotating at the same frequency. We move them to-

wards each other in real time by updating the respective trap minima and the position of the rotational axis of each condensate along the  $x$ -axis. Once the condensates merge at the center, we let the merged condensate evolve and analyze its behaviour. We also double the final rotation frequency compared to the initial ones. We investigate the nature of quantum turbulence and its associated incompressible kinetic energy spectra for rotating and non-rotating mergers under different merging times. We highlight the formation of dark solitons and how their dynamics are affected by rotation. Also, we examine the possibility of an adiabatic merger, where phase excitations and the suppression of subsequent formation of compressible sound waves in both rotating and non-rotating cases.

The paper is structured as follows. In Sec. II, we discuss the model used for the simulation and the governing equations for studying the condensate dynamics. We also mention the condensate parameters used in these simulations. Sections III A and III B elucidate the numerical results of merging non-rotating and rotating condensates, respectively. Finally, we summarize the results and present our conclusions and outlook in Sec. IV.

## II. MEAN-FIELD MODEL AND SIMULATION DETAILS

We consider a quasi-two-dimensional condensate with strong confinement along the  $z$ -axis with rotating frequency  $\Omega$ . The dynamical model describing a system of two condensates is given by the following Gross-Pitaevskii (GP) equation

$$i\frac{\partial\psi}{\partial t} = \left[ -\frac{1}{2}\nabla^2 + V(\mathbf{r}, t) + g_{2D}|\psi|^2 - \Omega(t)L_z \right] \psi, \quad (1)$$

where  $\psi \equiv \psi(\mathbf{r}, t)$  denotes the condensate wave function, with  $\mathbf{r} \equiv (x, y)$ ,  $\nabla^2$  is the two-dimensional Laplace operator defined as  $\nabla^2 \equiv \partial_x^2 + \partial_y^2$ , and  $V(\mathbf{r})$  is the external potential, which includes the harmonic trap along with the central circular barrier. The nonlinear term  $g_{2D} = 4\pi aN/(\sqrt{2\pi}d_z)$  represents the interaction strength between the atoms, where  $N$  is the total number of atoms,  $a$  is the s-wave scattering length, and  $d_z$  corresponds to the axial width of the trap. Here,  $\Omega(t)$  represents the rotational frequency, and  $L_z = i\hbar(y\partial_x - x\partial_y)$  is the  $z$  component of angular momentum.

In Eq. (1), the unit length is measured in terms of the transverse harmonic oscillator length  $l_{\text{ho}} = \sqrt{\hbar/(m\omega)}$ , time is measured in units of  $\omega^{-1}$ , and trap frequency is measured in terms of  $\omega$ , where,  $\omega$  is the transverse trap frequency. For both rotating and non-rotating cases, we fix  $N = 10^4$  and  $g_{2D} = 400$ . For the above choices of parameters, we obtain a scattering length of  $a \approx 3.8a_0$ . The BECs should have a strong axial confinement along  $z$  axis so as to restrict the dynamics within the  $x - y$  plane by implementing trap frequencies  $\omega_x \sim 2\pi \times 33\text{Hz}$ ,

$\omega_y \sim 2\pi \times 33\text{Hz}$ ,  $\omega_z \sim 2\pi \times 1.5\text{kHz}$ . This configuration provides a trap frequency of  $\omega = (\omega_x\omega_y\omega_z)^{1/3} \sim 2\pi \times 117.8\text{Hz}$ , harmonic oscillator length  $l_{\text{ho}} \approx 1\mu\text{m}$  and unit time  $\omega^{-1} \approx 1.3\text{ms}$ . The oscillator length along the  $z$  direction would be  $l_z \approx 0.28\mu\text{m}$ . Experimentally, for a condensate of  $^{87}\text{Rb}$  atoms, the desired scattering length can be accessible by tuning the magnetic fields utilizing the Feshbach resonance [42, 43].

To demonstrate the merger of the separated harmonic traps, we utilize the potential model and merging profile prescribed by Buchmann *et al.* [26]. The potential is given by

$$V(\mathbf{r}, t) = \frac{1}{2} [\gamma(|x| - s(t)l)^2 + \nu y^2], \quad (2)$$

where,  $\gamma = 1$  and  $\nu = 1$  are trap aspect ratios,  $l = 6.4$  is the initial position of the trap minimum. The function  $s(t)$  determines the merging time  $t_m$  which is defined as

$$s(t) = \begin{cases} \cos^2\left(\frac{\pi t}{2t_m}\right), & \text{if } 0 \leq t < t_m, \\ 0, & \text{if } t > t_m. \end{cases} \quad (3)$$

Initially, at  $t = 0$ , the traps are well-separated with their minima located at  $\pm l$ , where  $l$  is chosen large enough to prevent the condensate wavefunctions from overlapping. During the merging process, for  $0 < t < t_m$ , we allow the traps to move towards each other. The time evolution of the trap movement is characterized by the positions of the trap minima, denoted by  $\pm s(t)l$ . As the condensates approach each other, the barrier between them reduces, and subsequently, at the end of merging, there is a complete overlap between the two condensates. In the entire duration after the complete merging, i.e.,  $t > t_m$ , the condensate remains trapped within a single harmonic well.

To characterize the turbulence generated in the condensate due to the complex vortex dynamics, we perform a detailed analysis of the kinetic energy spectra and corresponding fluxes at different length and time scales. For this analysis, we decompose the kinetic energy into compressible and incompressible components [44] by transforming incompressible and compressible velocity fields into  $k$  space integrals via Parseval's theorem. We use the numerical implementation developed by Bradley and colleagues [45], which evaluates these integrals using the angle-averaged Wiener-Khinchin theorem as given below for the incompressible kinetic energy spectrum

$$\varepsilon_{\text{kin}}^i(k) = \frac{m}{2} \int d^2\mathbf{x} \Lambda_2(k, |\mathbf{x}|) C[\mathbf{u}^i, \mathbf{u}^i](\mathbf{x}), \quad (4)$$

where  $\varepsilon_{\text{kin}}^i(k)$  is the angle-averaged incompressible kinetic energy spectrum,  $\Lambda_2(k, |\mathbf{x}|) = (1/2\pi)kJ_0(k|\mathbf{x}|)$  is the 2D kernel function, involving the Bessel function  $J_0$  and  $C[\mathbf{u}^i, \mathbf{u}^i](\mathbf{x})$  represents the two-point auto-correlation function in position for a given incompressible velocity field. The above relation implies that for any of the position-space fields, there exists a spectral density

[see Eq. (4)] equivalent to an angle-averaged two-point correlation in  $k$  space.

To quantify the detailed nature of the internal structure and associated dynamics of a merged condensate, we calculate the average force exerted by one condensate on the other. For this, we compute the condensate momentum,  $\hat{P} = \psi^* (-i\nabla_{\perp}) \psi$ , where  $\psi$  is the condensate wave function and  $\nabla_{\perp} \equiv (\partial_x, \partial_y)$  is the two-dimensional gradient operator, which is then transformed to an angle-averaged Fourier integral. The spatial average of momentum in Fourier space is performed over the range  $k = 2\pi/R_{\text{TF}}$  to  $k = 2\pi/\xi$  where  $R_{\text{TF}}$  and  $\xi$  are the Thomas-Fermi radius and healing length of the condensate respectively. The forcing is given as the rate of change of the spatial average of momentum  $\tilde{f}(t) = \frac{d\langle \hat{P} \rangle}{dt}$  [34], where  $\langle \cdot \rangle$  denotes the spatial average.

### III. NUMERICAL RESULTS

To study the merging process, we numerically solve the dynamical Gross-Pitaevskii (GP) equation (1) using the split-Step Crank-Nicolson method [46–49]. Our simulations are performed on a spatial grid of size  $512 \times 512$  with space steps  $dx = dy = 0.05$  and time step  $dt = 10^{-4}$  to ensure convergence and accuracy. Similar to our previous work [50], the initial ground state consisting of two separate condensates is prepared using the imaginary time propagation scheme. Subsequently, we allow the merging of the condensates using the protocol discussed in the previous section, handled numerically using the real-time scheme for both rotating and non-rotating cases.

In the following section, we investigate different instabilities in both the rotating and non-rotating cases, including the appearance of vortices in the merged condensate, which ultimately drive the system towards turbulence. Subsequently, we characterize the turbulent fluctuations within the merged condensate by analyzing the kinetic energy spectra. Additionally, we analyze the influence of rotation on the formation and long-term evolution of vortices and solitons after the merging process and the conditions necessary for the onset of turbulence.

#### A. Dynamical instabilities and turbulence of the merged condensate without rotation

To begin with, we consider the merging dynamics of the condensate without any rotation. In this case, we prepare the initial state with a sufficient spatial separation between the two condensates to avoid any overlap between them. For a systematic investigation, we consider different merging times, viz.,  $t_m = 4, 6, 10$ , and  $20$  between the condensates, and subsequently characterize their ensuing instabilities and turbulence states. Here, we have excluded the cases with lower merging times, such as  $t_m < 4$ , because, for those events, the resulting condensate starts coming out from the single-well confinement

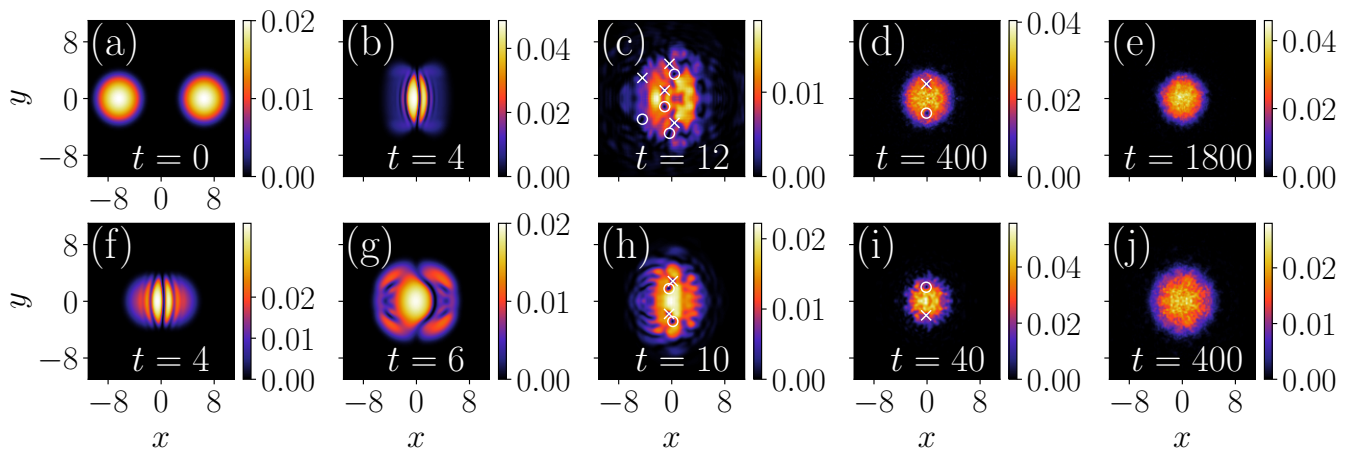


FIG. 1. Snapshots of the condensate density at (a)  $t = 0$ , and at different instances for merging times  $t_m = 4$  [(b) - (e)] and  $t_m = 6$  [(f)-(j)]. (b) shows the formation of interference fringes alongside a central soliton, (c)-(d) shows the formation of vortex-antivortex pairs, and (e) represents the snapshot after the vortex pair has annihilated. (f) indicates the formation of interference fringes, (g) soliton with significant bending, (h)-(i) formation of vortex pairs, and (j) subsequent annihilation. The anti-vortices and vortices are marked with cross ( $\times$ ) and circle ( $\circ$ ) symbols, respectively.

due to the presence of uncontrolled large excitations induced in them. This situation prevents the condensate from exhibiting systematic energy spectra scalings, even over short intervals. We choose  $t_m$  based on the rich dynamical instabilities inherited by the merged condensate, including the appearance of topological defects like vortices and their subsequent dynamics leading to the turbulent state.

In Fig. 1, we show the evolution of the condensate density profiles at different instants of time for merging time  $t_m = 4$  and  $t_m = 6$  in the top [Figs. 1(a)-1(e)] and bottom panels [Figs. 1(f)-1(j)], respectively. For  $t_m = 4$ , we notice the appearance of many intricate interference fringes, particularly a centralized dark soliton [panel(b)], which remains sustained in the newly formed single harmonic trap. However, as we follow up the dynamics for a longer duration, we find that the solitonic state does not remain stable, and they quickly get disintegrated into the combination of vortex-antivortex [panel (c)] pair as a result of the Snake instability [51–53]. Later, the vortex pair annihilates, generating compressible sound waves, as shown in panel (d). Additionally, compared to the density profiles observed at a slower merging time, we also observe the presence of interference fringes for the merging time  $t_m = 6$  [see Figs. 1(e)-(h)]. However, in this case, the soliton gets generated immediately after complete merging that exhibits significant bending [panel (f)], followed by a relatively quicker breakdown into vortex-antivortex pairs [panel (g)]. This particular feature triggers faster annihilation in the merged condensate compared to that of the  $t_m = 4$  case. For instance, for  $t_m = 6$  the condensates show a vortex-less state as a result of the vortex-antivortex annihilation even at  $t \sim 400$ , which was  $t \sim 1800$  for  $t_m = 4$ .

Our analysis reveals that the merging time signifi-

cantly affects the overall dynamics and structures of the merged condensate as the condensate transitions from the double well to the single well. To effectively capture this behaviour, Fig. 2 presents the temporal evolution of the condensate’s mean root-mean-squared radius ( $\langle r \rangle_{rms}$ ) for various merging times. For small merging

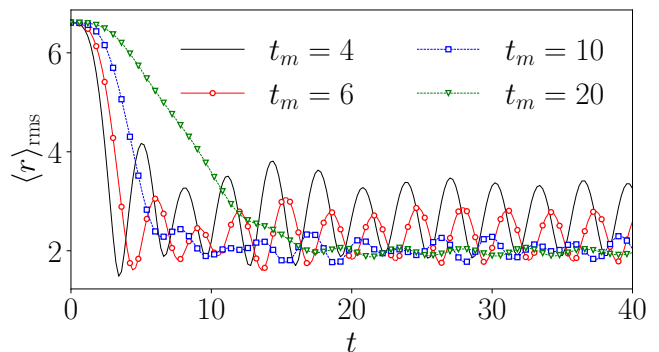


FIG. 2. Root mean square (rms) value of condensate radius as a function of time. The profile exhibits oscillations consistent with a frequency of  $2\omega$ , where  $\omega$  is the trap frequency.

time ( $4 \lesssim t_m \lesssim 6$ ), the merging condensate undergoes density oscillations with a frequency of  $2.0\omega$ . However, for longer merging time  $t_m \gtrsim 6$ , these oscillations subside.

Next, we calculate the instantaneous forcing to understand the role of different competing factors involved in the instabilities of the merged condensate during various merging times. This forcing, being the time derivative of the space-averaged density spectra, reflects the appearance of sharp discontinuities in the condensate density at a specific time. Additionally, a finite jump in the force indicates the emergence of soliton formation [26]. Fig-

ure 3(a) illustrates the time evolution of the forcing for different merging times. It shows a decrease in forcing peak amplitude with longer merging times. This could potentially indicate phase discontinuities caused by the presence of solitons, which subsequently become less pronounced for larger merging times. The forcing peaks also decrease over time for a given merging time as the solitons eventually decay. Furthermore, the temporal evolution of the force exhibits an oscillation with a frequency of  $2\omega$  which can be attributed to the presence of the harmonic trap with frequency  $\omega$ . These oscillations in the forcing value can be further related to the solitons bouncing off the trap boundary and propagating in the opposite  $x$ -direction. The phase profiles in Figs 3(b)-(e) highlight

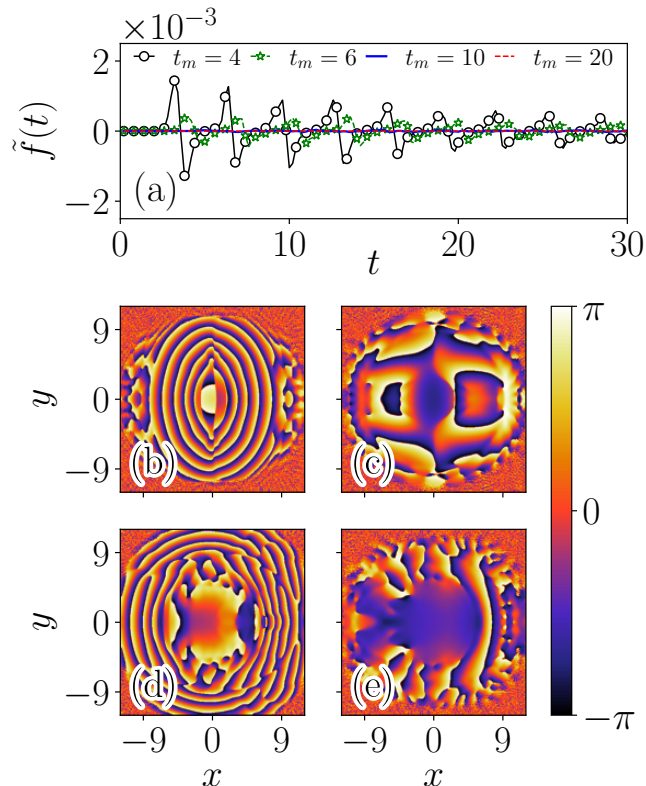


FIG. 3. (a) Temporal evolution of the forcing term  $f$  with non-rotating case for different merging times:  $t_m = 4$  (black solid line with empty squares),  $t_m = 6$  (green line with circles),  $t_m = 10$  (blue solid line), and  $t_m = 20$  (red dashed line). Condensate phase profiles at the time of merger for various merging times (b)  $t_m = 4$ , (c)  $t_m = 6$ , (d)  $t_m = 10$  and (e)  $t_m = 20$ .

the variation in soliton profiles with respect to merging time. For faster mergers, we observe a larger number of solitons with sharper phase jumps [cf. Fig. 3(b)]. In contrast, slower mergers result in fewer solitons with smoother phase jumps [cf. Figs. 3(c)-(e)]. The soliton velocity depends on the phase difference across the soliton [33]. A larger phase jump indicates a narrow and deep soliton moving slowly, while a smoother phase gradient signifies a wider and shallower soliton moving closer

to the speed of sound.

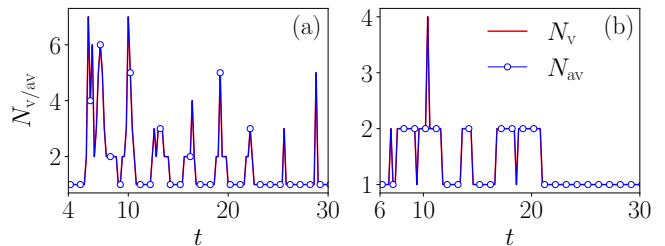


FIG. 4. Evolution of vortex ( $N_v$ ) and anti-vortex ( $N_{av}$ ) numbers within the Thomas-Fermi radius of the condensate ( $R_{TF}$ ) for (a)  $t_m = 4$ , (b)  $t_m = 6$ . No vortices are observed for higher merging times.

To further analyze the mechanism responsible for the decay of solitons into vortex pairs, we investigate the temporal profile of the angular momentum and vortex number for  $t_m = 4$  and 6, as depicted in Fig. 4. An early increase in angular momentum suggests the formation of point vortices due to the breaking of solitons in the non-rotating condensate. We then observe a subsequent decrease, indicating the annihilation of vortex-antivortex pairs. For longer merging times, the angular momentum peak appears earlier and decreases more rapidly, suggesting earlier soliton decay into vortex pairs and their subsequent annihilation.

One may witness strong evidence of soliton decay for different merging times in the vortex numbers illustrated in Fig. 4, where populations of vortices and anti-vortices appear to be equal for both merging times. The oscillations in the vortex number can be attributed to density oscillations, which are more pronounced for faster mergers ( $t_m = 4, 6$ ).

Furthermore, evidence suggests the formation of dark neutral lumps (vortexoniums) from the coalescence of vortices and anti-vortices [51, 54, 55]. These vortex pairs undergo a cyclical process of forming lumps and returning to vortices until the vortexonium dissipates into compressible excitations. For longer merging times, the soliton becomes wide enough to reach the sound velocity before complete condensate merging. This results in dissipation without exhibiting snake instability, explaining the absence of vortex pairs in such cases.

Next, we analyze the incompressible and compressible kinetic energies, which offer insights into the detailed nature of the fluctuations generated during the merging process, thereby quantifying the different characteristics of the merged condensate. The presence of point vortices contributes to the incompressible kinetic energy, whose evolution follows a similar trend as that of angular momentum and vortex numbers. The compressible kinetic energy also exhibits an early peak due to the trap merger generating sound waves, which eventually diminish and settle as the merged condensate evolves. Notably, the compressible kinetic energy is comparable to the incompressible kinetic energy due to the smaller number of vor-

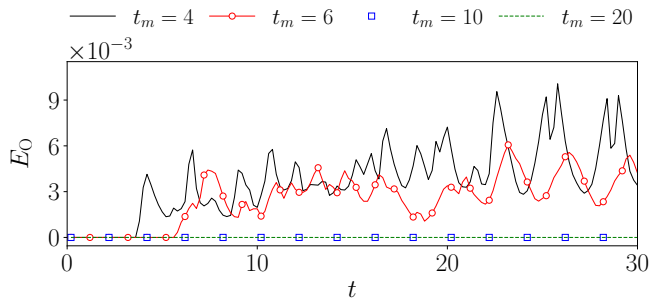


FIG. 5. Evolution of Onsager energy  $E_O$  with respect to time for the non-rotating case for merging times  $t_m = 4$  (black solid line),  $t_m = 6$  (red line with empty circles),  $t_m = 10$  (blue squares),  $t_m = 20$  (green dashed line).

tices.

The Onsager energy,  $E_O$ , i.e., the energy per vortex, is also computed and displayed in Fig. 5 for various merging times. The Onsager energy indicates that vortices formed through shorter mergers are more energetic and undergo oscillations consistent with a frequency  $2.0\omega$ .

Figures 6(a)-(d) illustrate the temporal evolution of the various energy components, such as the expectation value of the potential energy ( $E_{pot}$ ), interaction energy ( $E_{int}$ ), kinetic energy ( $E_{kin}$ ), rotational energy ( $E_{rot}$ ) for different merging time  $t_m = 4, 6, 10$ , and  $20$ , respectively. We notice that the kinetic energy decays to zero

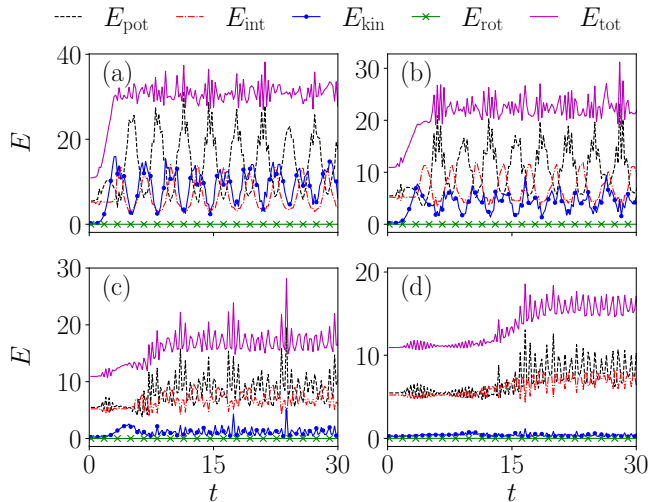


FIG. 6. Evolution of different components of condensate energies with respect to time for (a)  $t_m = 4$ , (b)  $t_m = 6$ , (c)  $t_m = 10$ , and (d)  $t_m = 20$ .

for longer merging times ( $t_m = 10, 20$ ), indicating that the merger is quasi-static for these  $t_m$ . Further, we find that the total energy gets significantly reduced as merging time increases, indicating a decrease in the excitation energy. This excitation energy depends on the depth of dark solitons, which are shallower for the slower merging

cases, as shown in Fig. 6. A point to note is that all these time-varying quantities display oscillations with a frequency of  $2.0\omega$  due to the nature of harmonic confinement. However, these oscillations get reduced when the merging reaches the quasi-static regime where the merger is slow enough not to instigate any dynamical process. These mergers appear to be the same as adiabatic mergers [26].

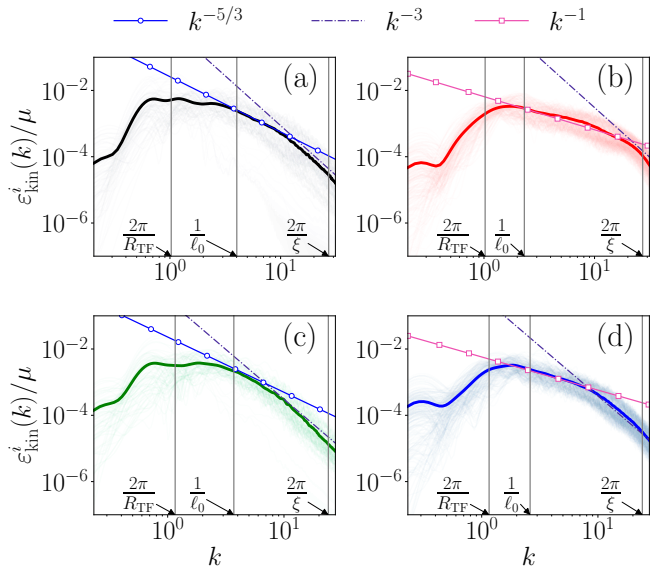


FIG. 7. Time-averaged incompressible kinetic energy spectra for the non-rotating case, for merging time  $t_m = 4$  in the time range (a)  $t = 4$  to  $t = 20$  (b)  $t = 20$  to  $t = 40$  and for merging time  $t_m = 6$  in the time range (c)  $t = 6$  to  $t = 20$  and (d)  $t = 20$  to  $t = 40$ . Both merging cases initially show  $k^{-5/3}$  scaling and later a  $k^{-1}$  scaling.

Next, to understand the detailed nature of the turbulence for different merging times, in Fig. 7, we present the incompressible kinetic energy spectra for various merging times. We observe that the merging condensate, except for the  $t_m = 4, 6$  cases, does not exhibit any scaling behaviour in the inertial range. Additionally, the merged condensate immediately after merging ( $t_m = 4, 6$ ) displays a  $k^{-5/3}$  scaling for length scales smaller than the inter-vortex distance,  $\ell_0$ . This differs from the case where turbulence appears in a single condensate, as reported in Ref. [50]. This behaviour can be attributed to the dominance of single vortex dynamics and the lack of sufficient vortices to display a clear Kolmogorov-like cascade of energy. However, at later times (significantly longer than the merging time), the condensate displays  $k^{-1}$  scaling at regions smaller than the inter-vortex distance, indicating a Vinen-like cascade [50, 56, 57]. These scaling behaviours exhibited by the merged condensate are generally short-lived due to the annihilation of vortices in the absence of external mechanisms to generate new vortices, such as rotation. These features are also evident in the absence of a forcing peak at smaller  $k$  values, indicating

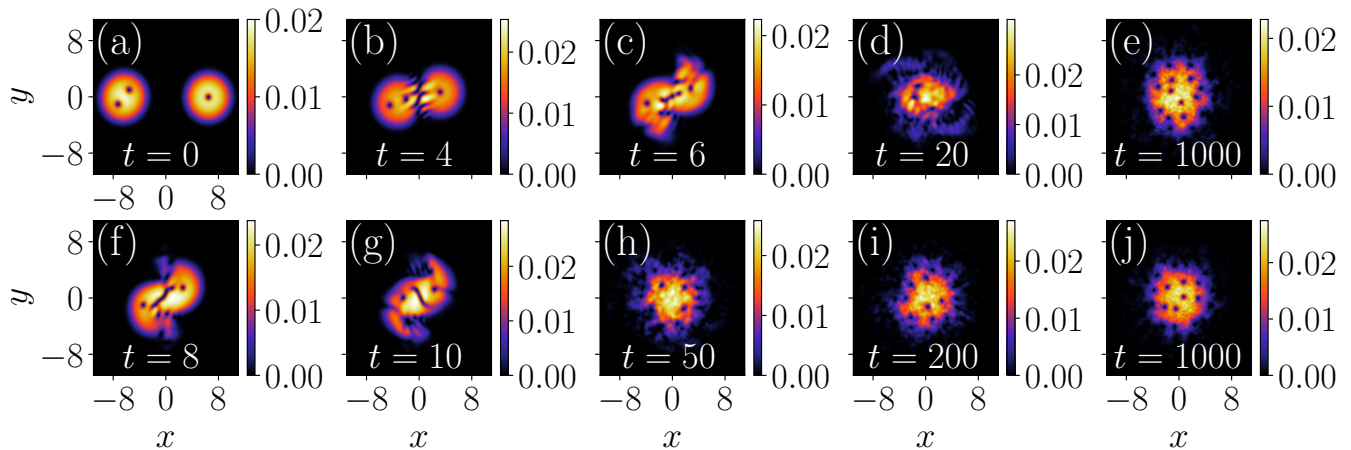


FIG. 8. Snapshots of the condensate density at (a)  $t = 0$  and at different instances during the condensate merger for merging times  $t_m = 6$  [(b) - (e)] and  $t_m = 10$  [(f)-(j)]. (b) Off-axis collisions forming weaker bent soliton structures, (c) soliton vortex interactions, (d)-(e) formation of single harmonically confined condensate with a vortex lattice, (f)-(g) shows off-axis collision with soliton-vortex interaction, and (h)-(j) appearance of the vortex lattice in the merged condensate.

a lack of a proper mechanism to sustain the turbulent fluctuations in the merged condensate.

### B. Effect of rotation on the dynamics and turbulence state of the merged condensate

Having a comprehensive insight into the merger of two non-rotating condensates, we now turn our attention to investigating the effect of rotation on the merging dynamics of the condensate, starting with a low frequency of ( $\Omega = 0.45$ ). Similar to the non-rotating case for this case as well we achieve the merger by moving the traps and their rotating axes towards each other along the  $x$ -axis and simultaneously increasing their frequencies at the same rate, resulting in a final merged condensate rotating at  $\Omega = 0.9$ .

In Figs. 8, we present the snapshots of the condensate at different instants of time for  $t_m = 6$  [8(a)-(e)] and  $t_m = 10$  [8(f)-(j)]. We notice that the condensates undergo an off-axis merger, deviating from the purely along-the- $x$ -axis behaviour seen in the non-rotating case. This off-axis nature, arising from the movement of the rotation axis and trap towards the center of the simulation domain, becomes more pronounced for larger initial separations and shorter merging times ( $t_m = 6, 10$ ). In such cases, the condensates can potentially spiral into each other, which strongly influences the nature of the soliton that appears as results of the instability, leading to distortions and orientation at an angle to the  $x$ -axis due to the presence of rotation. Soliton-vortex interactions also become more probable for slower mergers (see Fig. 8 bottom panel), but compared to the situation as discussed in [33], these interactions do not affect the vortex numbers or angular momenta in presence of the rotation.

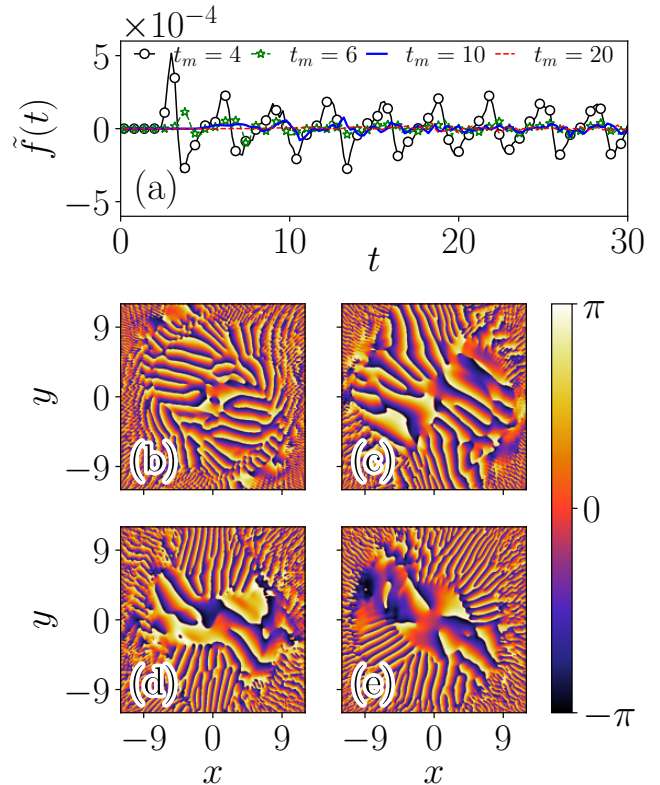


FIG. 9. (a) Temporal evolution of the forcing term  $f$  with rotating case for different merging times:  $t_m = 4$  (black solid line with empty squares),  $t_m = 6$  (green dashed line with circles),  $t_m = 10$  (blue solid line), and  $t_m = 20$  (red dashed line). Condensate phase profiles at the time of merger for various merging times: (b)  $t_m = 4$ , (c)  $t_m = 6$ , (d)  $t_m = 10$  and (e)  $t_m = 20$ .

Next, we show the temporal evolution of the forcing of the merged condensate in Fig. 9(a) for different  $t_m$ , which follows a similar pattern to that of the non-rotating case but has a significantly smaller forcing amplitude due to the presence of shallower solitons that exhibit significant bending. Notably, the amplitude decays much slower when compared to the non-rotating case and persists for longer times due to the presence of rotational effects. The phase profiles in Figs 9(b)-(e) illustrate the nature of the soliton at the instant when merging takes place for  $t_m = 4, 6, 10,$  and  $20$  respectively for the rotating condensate. For small merging times ( $t_m = 4, 6$ ), we notice the presence of a large number of solitons, which are quite evident from the discontinuous phase jumps [cf. Fig. 9(b,c)]. Conversely, for  $t_m = 10, 20$ , the phase profile is smoother, indicating the presence of fewer solitons and the emergence of vortices [cf. Figs. 9(d)-(e)]. Similar to the non-rotating case, we can relate the large velocity jump to the high velocity of the soliton, while the smooth phase corresponds to the soliton moving with the sound velocity [33]. To characterize the effect of the rotation

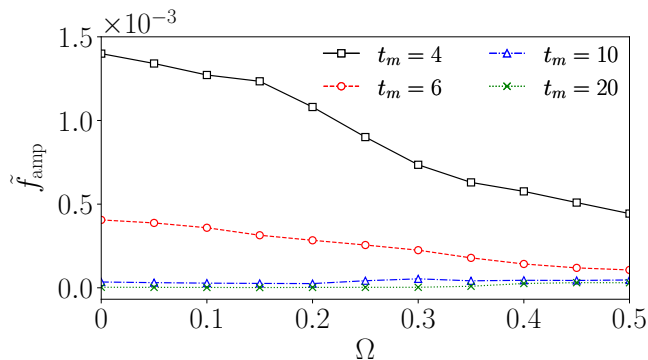


FIG. 10. Variation of forcing amplitude against the rotating frequency for different merging times of  $t_m = 4, t_m = 6, t_m = 10,$  and  $t_m = 20$ .

frequency on the force amplitude, which in turn affects the structure and dynamics of the soliton. In Fig. 10, we depict the variation of the force amplitude ( $f_{amp}$ ) with the angular frequency ( $\Omega$ ) of the rotation for different  $t_m$ . We find that for small merging times ( $t_m = 4, 6$ ), the force amplitude decreases with an increase in  $\Omega$ . However, for longer merging times ( $t_m = 10, 20$ ), the force amplitude is close to zero and independent of  $\Omega$ .

The angular momentum shows a significantly higher vortex count at shorter merging times. This phenomenon arises from the formation and subsequent decay of solitons into vortex-antivortex pairs, contributing to the angular momentum in cases where  $t_m = 4, 6$ . For longer merging times, the likelihood of soliton formation diminishes, resulting in a decrease in the contribution of solitons to both angular momentum and vortex numbers. Additionally, the rotational effect causes the vortex population to surpass the anti-vortex population. Figure 11 illustrates the evolution of vortex numbers over time. No-

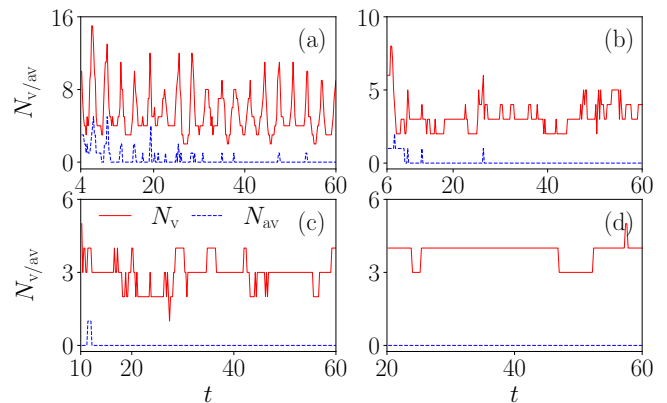


FIG. 11. Evolution of vortex ( $N_v$ ) and anti-vortex ( $N_{av}$ ) numbers within the Thomas-Fermi radius of the condensate ( $R_{TF}$ ) for (a)  $t_m = 4$  (b)  $t_m = 6$  (c)  $t_m = 10$  (d)  $t_m = 20$  for rotating case with  $\Omega = 0.45$ .

tably, the presence of rotation leads to significantly more vortices than anti-vortices, and the existence of vortex pairs confirms soliton decay. For faster mergers in Figure 11(a), the vortex number oscillates at  $2\omega$  due to density oscillations. However, we witness a significant reduction of this behaviour for slower mergers in Figs. 11(c)-(d), following a trend similar to the previous case.

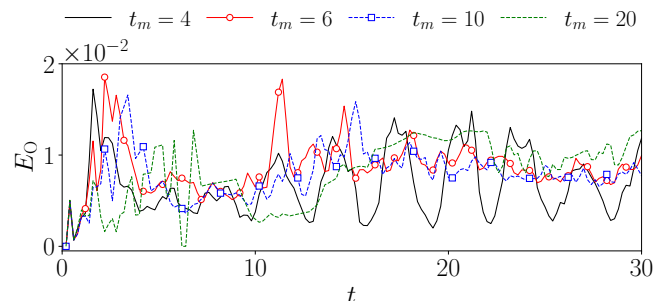


FIG. 12. Evolution of Onsager energy  $E_O$  with respect to time for the non-rotating case for merging times  $t_m = 4$  (black solid line),  $t_m = 6$  (red solid line with empty circles),  $t_m = 10$  (blue dashed line),  $t_m = 20$  (green dashed line with empty squares).

The incompressible kinetic energy evolution exhibits a decreasing trend concerning merging time. In contrast to the non-rotating scenario, the incompressible energy does not quickly settle down. Instead, it persists alongside the angular momentum profiles, indicating a continuous production of vortices. Examining the compressible kinetic energy reveals a trend similar to that of the non-rotating case. However, for longer merging times ( $t_m = 20$ ), there is a persistent and constant compressible energy, while in the non-rotating case, the compressible energy approaches zero at these times. This discrepancy is primarily due to the presence of rotational forcing, which not only generates more vortices but also enhances the production of compressible sound waves. The Onsager

energy profile for different merging times in the rotating case is quite different, as shown in Fig. 12. In the rotating case, vortices are not only formed via decaying solitons but also due to the presence of rotation. From Fig. 12 one can see that vortices formed via rotation have more Onsager energy when compared to the ones formed via solitons. The lowest Onsager energy for  $t_m = 4$  (black line) can be attributed to the significant increase in the number of vortices formed due to snake instability, that lowers the overall Onsager energy in the condensate despite the presence of vortices formed due to rotation.

In Fig. 13(a)-(d), we show the various energy components,  $E_{pot}$ ,  $E_{int}$ ,  $E_{kin}$ ,  $E_{rot}$  for different merging times, i.e.,  $t_m = 4, 6, 10,$  and  $20$ , respectively, keeping the rotation frequency fixed at  $\Omega = 0.45$ . Similar to the non-

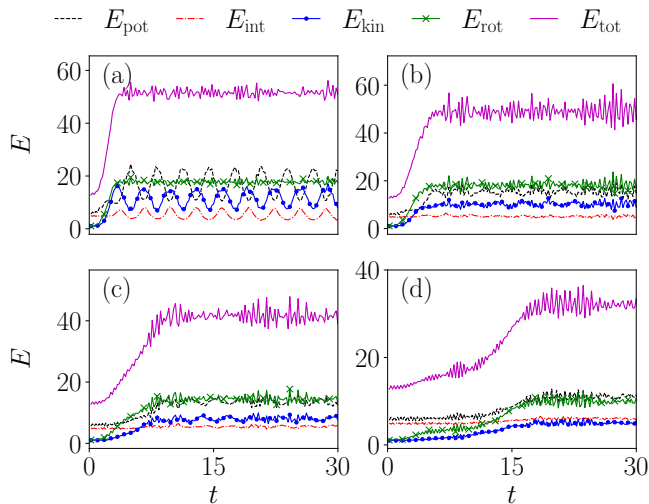


FIG. 13. Evolution of different components of condensate energies with respect to time for (a)  $t_m = 4$ , (b)  $t_m = 6$ , (c)  $t_m = 10$ , and (d)  $t_m = 20$  for rotating case with  $\Omega = 0.45$ .

rotating case, all energy components (except for rotation energy) exhibit oscillations consistent with the trap frequency for shorter merging times. However, unlike the non-rotating case, the amplitude of these oscillations damps out quickly [cf. Figs. 13(b)-(d)]. The kinetic energy decreases with increasing merging time, but unlike the non-rotating merger, it does not go to zero for the  $t_m = 10$  and  $t_m = 20$  cases.

Achieving an adiabatic merger in the condensate depends on both the merging time ( $t_m$ ) and the rotation frequency ( $\Omega$ ), as shown in Fig. 14. Condensates rotating at frequency  $\Omega$  merge to form a condensate rotating at  $2\Omega$ . Sufficiently long merging times ensure that this merged condensate reaches its ground state. Notably, for both non-rotating condensates and those at low rotation frequencies [black line with empty squares in Fig. 14(a)], the ground state is achieved with merging times of  $t_m \sim 20$ . In Figs. 14(b), as rotation frequency increases, longer merging times are required for the final condensate to approach its ground state. Even without

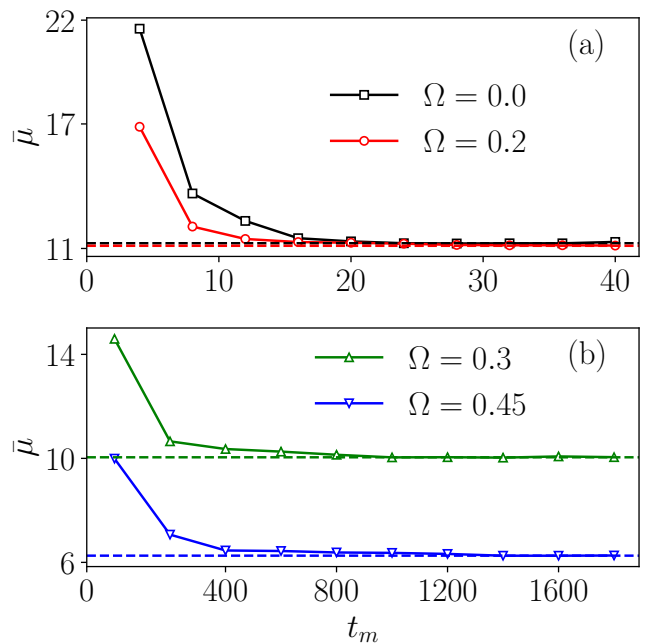


FIG. 14. Evolution of chemical potential (averaged over 3000 time units from the time of merger) of the merged condensate with respect to different merging times for (a)  $\Omega = 0.0$  (black line with empty squares) and  $\Omega = 0.2$ , (red line with empty circles) and (b)  $\Omega = 0.3$  (green line with empty triangles) and  $\Omega = 0.45$  (blue line with empty triangles) frequencies, respectively. The dashed horizontal lines represent the ground state chemical potential for the merged condensate rotating at  $2\Omega$ .

soliton decay, trap movement can create compressible excitations. These excitations persist longer at higher rotation frequencies, as rotational forcing prevents them from dissipating, thus requiring much slower mergers to suppress them.

The incompressible kinetic energy spectra for the rotating case exhibit similar scaling behaviour to that of the non-rotating case (see Fig. 15). It is important to note that a forcing peak emerges due to rotation at  $k < 2\pi/R$  gradually diminishes for longer merging times. For cases with  $t_m = 4$  and  $t_m = 6$ , a short-lived  $k^{-5/3}$  scaling is initially observed, which later transforms into a  $k^{-1}$  scaling, corresponding to the formation of vortex-rings (see Ref. [58]). These vortex rings are formed in the soliton decay process through snake instability, as illustrated in Ref. [51].

In contrast to the non-rotating case, where no scaling is observed for  $t_m = 10$  and  $t_m = 20$ , the rotating case exhibits  $k^{-5/3}$  scaling, albeit for a relatively shorter  $k$  range initially. However, the  $k^{-1}$  scaling persists for the  $t_m = 10$  case but not for the  $t_m = 20$  case, as no soliton is formed to decay into vortex-rings. In the non-rotating scenario, the scaling behaviour of the incompressible spectra disappears due to vortex annihilation. Also, in contrast to the non-rotating case, the  $k^{-5/3}$  scaling appears consistently for length scales larger than

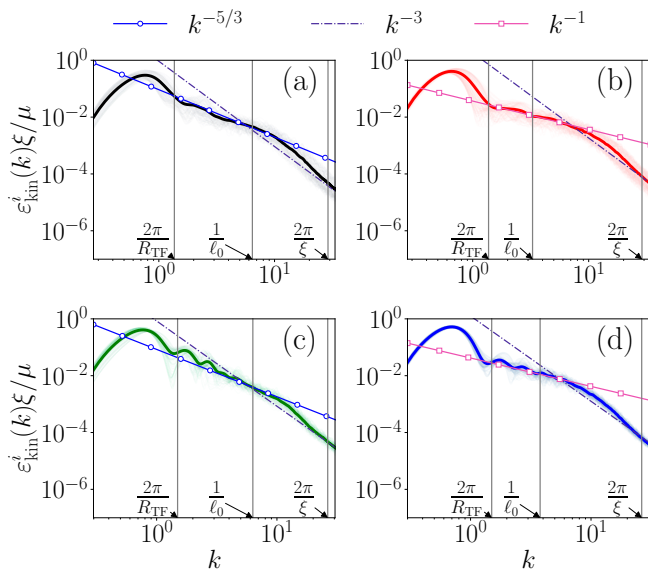


FIG. 15. Time-averaged incompressible kinetic energy spectra for the rotating case ( $\Omega = 0.45$ ), for merging time  $t_m = 4$  in the time range (a)  $t = 4$  to  $t = 24$  (b)  $t = 24$  to  $t = 44$  and for merging time  $t_m = 6$  in the time range (c)  $t = 6$  to  $t = 26$  and (d)  $t = 26$  to  $t = 46$ . Both cases initially showing  $k^{-5/3}$  and later a  $k^{-1}$  scaling.

inter-vortex distance  $\ell_0$ , where collective vortex dynamics dominate and hence display Kolmogorov cascade. This is due to rotational effects introducing a significant number of vortices in the condensate, enabling their collective behaviour. This is possible frequencies above a critical frequency  $\Omega > \Omega_c$  [49], which in our case is  $\Omega_c \sim 0.3$ . Similarly, the  $k^{-1}$  scaling also appears at smaller length scales where single-vortex dynamics dominate, clearly indicating Vinen-like turbulence. In the presence of sustained rotation, we observe a more pronounced Kolmogorov cascade of  $k^{-5/3}$  at smaller  $k$  regions after at longer times. This phenomenon closely resembles the later stage evolution of rotating condensates, as previously studied in [50].

#### IV. CONCLUSION

We have numerically investigated the merging dynamics of Bose-Einstein condensates with random phases confined in harmonic traps, analyzing the impact of rotation on the process. Initially, we studied mergers without rotation for various merging times. All exhibited consistent scaling behaviour in the incompressible kinetic energy spectra. Density profiles at different merging times showed the formation of dark solitons due to interference patterns generated by condensate overlap. Notably, interference fringes closer to the minima of the final trap persisted longer than those near the boundaries. These dark solitons exhibited bending and subsequently de-

cayed into vortex pairs via snake instabilities. Vortex-antivortex pairs eventually annihilated after multiple rebounds within the trap. However, while observing these features for all merging times ( $t_m = 4, 6, 10,$  and  $20$ ), the nature of the dark solitons, their instability-driven behaviour, and the phenomenon's timeframe varied significantly. Increasing the merging time resulted in a decrease in the depth and size of the central dark soliton. Since soliton depth influences phase excitations, slower merging led to the attainment of the BEC's ground state. This depth decrease was confirmed by analyzing the time-dependent variation of the forcing term. Furthermore, the angular momentum, vortex number, and incompressible kinetic energy density profiles provided temporal evidence of vortex formation and annihilation. This process occurs relatively quickly for faster mergers. The compressible kinetic energy, indicating sound waves from phase excitations, also showed a decreasing trend and almost disappeared for longer merging times. All energy profiles displayed oscillations with frequency twice that of the trap ( $2\omega$ ) due to phase excitations. These naturally subsided and disappeared for slower mergers. In the beginning, the incompressible kinetic energy spectra exhibited  $k^{-5/3}$  but only at length scales where single vortex dynamics dominate, hence ruling out the Kolmogorov cascade. Later, for a short period, they transitioned to a  $k^{-1}$  scaling attributed to vortex rings formed from soliton breaking via the snake instability [58]. However, the absence of forcing in the non-rotating case prevented these scaling laws from persisting beyond vortex annihilation. The formation of vortices through merging BECs with random initial phases, even in the absence of rotation, agrees with conclusions drawn from Refs. [4, 26].

With rotation, the merging condensates display contrasting behaviour for identical merging times, consistent with observations without rotation. The evolution of the density indicates that the condensates merge off the  $x$ -axis despite the model restricting translational motion strictly along the  $x$ -axis, which results in them experiencing each other's rotational effects as they approach. It significantly weakens the resultant dark solitons and orients with an angle to the  $x$ -axis. These solitons also appear to interact with the pre-existing and newly formed vortices. After merging, their rotating frequencies combine, resulting in the final condensate rotating at twice the initial frequency of the individual condensates. The significantly lower amplitude of the time-dependent forcing term confirms the weak nature of the solitons compared to the non-rotating case. The angular momentum and incompressible kinetic energy profiles indicate continuous vortex production due to sustained rotation and compressible turbulence generation. The number of vortices exceeds the anti-vortex number due to the rotation's impact on the vortex population.

Although compressible kinetic energy exhibits a decreasing trend, it does not necessarily approach zero as rapidly for longer merging times, as observed in the non-rotating case. This finding, in conjunction with the av-

erage chemical potential plot, indicates that an adiabatic merger is feasible only for merging times exceeding  $t_m = 1000$ , unlike non-rotating cases where the merged condensate reaches the ground state by  $t_m = 20$ . While the resulting soliton is shallower and has a weaker influence on phase excitations, the rotational forcing significantly impacts the sound waves produced, which persist without dissipation. Notably, during adiabatic mergers in the rotating case, the quasi-static nature of the merger substantially reduces off-axis merging.

The incompressible kinetic energy spectra exhibit a scaling behaviour similar to that of the non-rotating case. However, these spectra display a forcing peak at  $k < 2\pi/R$ . Initially, the scaling range extends to length scales longer than the intervortex length  $k < 2\pi/\ell_0$  indicating the onset of Kolmogorov cascade and at later times displays Vinen-like turbulence. With sustained rotation over longer durations, we observe spectra similar to those presented in our previous work for the  $\Omega = 1$  case [50], where the Kolmogorov cascade is observed at smaller  $k$  values.

We have also carried out the simulations at various rotating frequencies and identified trends. At lower frequencies, both the scaling duration and ranges are significantly shorter, while the depth of the dark soliton is larger compared to higher rotation frequencies. Additionally, off-axis merging is less pronounced at lower frequencies. Despite these trends, the rotational case does not exhibit fundamental differences across various rotating frequencies to the same extent as the non-rotating case. Rotational merging presents interesting dynamics, particularly with large initial separations. In the case of off-axis motion, substantial separations can even lead to condensates spiralling into each other for faster merging times despite the model strictly moving the condensates along the  $x$ -axis.

The present study is also relevant for understanding the remnants of binary neutron-star merger event GW170817 [8, 9]. Theory predicts the aftermath of such an event should produce a stellar black hole, though observations fail to confirm this prediction conclusively. However, the following works in Refs. [10, 11], pulsars are most likely born with embryonic incompressible gluon-quark superfluid cores that become more massive as they evolve in cosmic times. During the merger, the low-energy entropy-free cores are predicted to fuse smoothly together, whereas the merger of surrounding envelopes of compressible and dissipative normal matter goes violently. Hence, the study may pave the way to explore the nature of gravitationally bound rotating BECs.

#### ACKNOWLEDGMENTS

The works of A.S. and P.M. are supported by MoE RUSA 2.0 (Bharathidasan University - Physical Sciences).

#### Appendix A: Compressible kinetic energies

In this appendix, we present the spatial configuration of the compressible kinetic energy for  $t_m = 4$ , which is useful to characterize the different sorts of instabilities appearing after the merging leading to the turbulent state for both rotating as well as non-rotating condensates. Upon observing the time evolution of the forcing

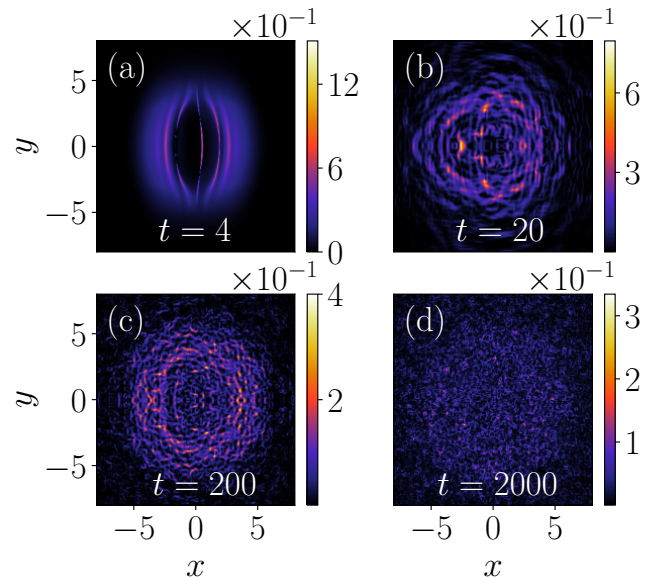


FIG. 16. Time evolution of compressible energy density for non-rotating condensates merging at  $t_m = 4$ .

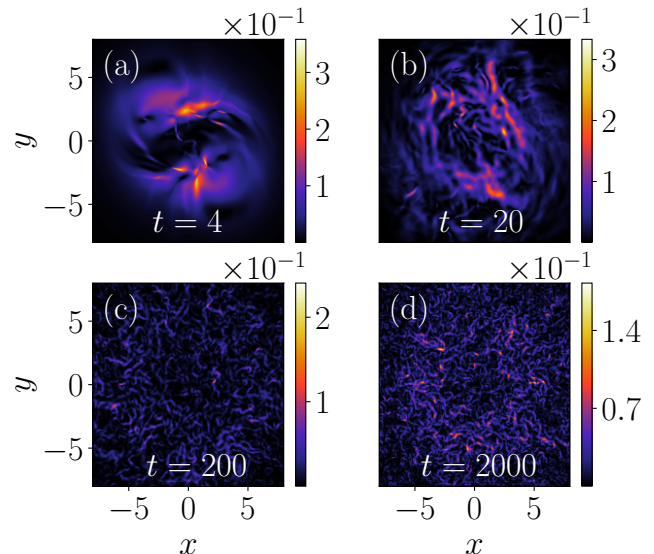


FIG. 17. Time evolution of compressible energy density for rotating condensates merging at  $t_m = 4$ .

term, we notice that the forcing amplitude decays relatively quickly for the non-rotating case compared to the

rotating one. Additionally, the forcing experienced in the condensate manifests as compressible energy generated in the merged condensate. We highlight this by analyzing the spatial density profiles of compressible kinetic energy. For the non-rotating case, we observe that the dark solitons contribute to the compressible energy density [see Fig. 16(a)]. Eventually, the energy becomes more evenly distributed and finally granulates at longer times [see Fig. 16(b)-(d)]. The decreasing amplitude of the energy density and the initial accumulation of compressible energy in solitons correlates with the evolution

of the forcing term. The energy density for the rotating case further confirms this correlation, as the energy amplitude is significantly lower and distributed over a wider soliton. Similar to the forcing amplitude decreasing at a slower rate, the compressible energy peaks also do not decay quite as fast as in the non-rotating case within the same time interval (see Fig. 17). It is also noteworthy that, compared to the non-rotating case, the compressible energy is distributed as strands and is more clumped at longer times. This spatial profile resembles the long-term evolution of compressible kinetic energy shown in rotational quantum turbulence [50].

- 
- [1] I. Bloch, T. W. Hänsch, and T. Esslinger, Atom laser with a cw output coupler, *Phys. Rev. Lett.* **82**, 3008 (2006).
- [2] M. R. Andrews, C. G. Townsend, H.-J. Miesner, D. S. Durfee, D. M. Kurn, and W. Ketterle, Observation of interference between two Bose condensates, *Science* **275**, 637 (1997).
- [3] G.-B. Jo, J.-H. Choi, C. A. Christensen, T. A. Pasquini, Y.-R. Lee, W. Ketterle, and D. E. Pritchard, Phase-sensitive recombination of two Bose-Einstein condensates on an atom chip, *Phys. Rev. Lett.* **98**, 180401 (2007).
- [4] D. R. Scherer, C. N. Weiler, T. W. Neely, and B. P. Anderson, Vortex formation by merging of multiple trapped Bose-Einstein condensates, *Phys. Rev. Lett.* **98**, 110402 (2007).
- [5] T. W. Kibble, Topology of cosmic domains and strings, *J. Phys. A* **9**, 1387 (1976).
- [6] W. H. Zurek, Cosmological experiments in superfluid helium?, *Nature* **317**, 505 (1985).
- [7] A. P. Chikkatur, Y. Shin, A. E. Leanhardt, D. Kielpinski, E. Tsikata, T. L. Gustavson, D. E. Pritchard, and W. Ketterle, A continuous source of Bose-Einstein condensed atoms, *Science* **296**, 2193 (2002).
- [8] B. Abbott, R. Abbott, T. Abbott, F. Acernese, K. Ackley, C. Adams, T. Adams, P. Addesso, R. Adhikari, V. Adya, *et al.* (LIGO Scientific Collaboration and Virgo Collaboration), Properties of the binary neutron star merger GW170817, *Phys. Rev. X* **9**, 011001 (2019).
- [9] B. P. Abbott, R. Abbott, T. Abbott, F. Acernese, K. Ackley, C. Adams, T. Adams, P. Addesso, R. Adhikari, V. B. Adya, *et al.* (LIGO Scientific Collaboration and Virgo Collaboration), GW170817: observation of gravitational waves from a binary neutron star inspiral, *Phys. Rev. Lett.* **119**, 161101 (2017).
- [10] A. A. Hujeirat and R. Samtaney, The remnant of GW170817: A trapped neutron star with a massive incompressible superfluid core, *J. Mod. Phys.* **11**, 1785 (2020).
- [11] A. A. Hujeirat and M. M. Wicker, Evidence for false vacuum states inside the cores of massive pulsars and the ramification on the measurements of their true masses, *J. Mod. Phys.* **14**, 1409 (2023).
- [12] B. Xiong, T. Yang, and K. A. Benedict, Distortion of interference fringes and the resulting vortex production of merging Bose-Einstein condensates, *Phys. Rev. A* **88**, 043602 (2013).
- [13] Y. Shin, M. Saba, T. A. Pasquini, W. Ketterle, D. E. Pritchard, and A. E. Leanhardt, Atom interferometry with Bose-Einstein Condensates in a double-well potential, *Phys. Rev. Lett.* **92**, 050405 (2004).
- [14] S. Stock, Z. Hadzibabic, B. Battelier, M. Cheneau, and J. Dalibard, Observation of phase defects in quasi-two-dimensional Bose-Einstein condensates, *Phys. Rev. Lett.* **95**, 190403 (2005).
- [15] H. Li, E. Halperin, S. Ronen, and J. L. Bohn, Merging dipolar supersolids in a double-well potential, *Phys. Rev. A* **109**, 013307 (2024).
- [16] D.-I. Choi, Collision of gravitationally bound Bose-Einstein condensates, *Phys. Rev. A* **66**, 063609 (2002).
- [17] E. Cotner, Collisional interactions between self-interacting nonrelativistic boson stars: Effective potential analysis and numerical simulations, *Phys. Rev. D* **94**, 063503 (2016).
- [18] A. Paredes and H. Michinel, Interference of dark matter solitons and galactic offsets, *Phys. Dark Universe* **12**, 50 (2016).
- [19] B. Schwabe, J. C. Niemeyer, and J. F. Engels, Simulations of solitonic core mergers in ultralight axion dark matter cosmologies, *Phys. Rev. D* **94**, 043513 (2016).
- [20] Y. Nikolaieva, Y. Bidasyuk, K. Korshynska, E. Gorbar, J. Jia, and A. Yakimenko, Stable vortex structures in colliding self-gravitating Bose-Einstein condensates, *Phys. Rev. D* **108**, 023503 (2023).
- [21] X. Zhang, M. H. Chan, T. Harko, S.-D. Liang, and C. S. Leung, Slowly rotating Bose Einstein condensate galactic dark matter halos, and their rotation curves, *Eur. Phys. J. C* **78**, 1 (2018).
- [22] J. A. Stickney and A. A. Zozulya, Influence of nonadiabaticity and nonlinearity on the operation of cold-atom beam splitters, *Phys. Rev. A* **68**, 013611 (2003).
- [23] A. Mebrahtu, A. Sanpera, and M. Lewenstein, Splitting and merging an elongated Bose-Einstein condensate at finite temperature, *Phys. Rev. A* **73**, 033601 (2006).
- [24] W. Yi and L.-M. Duan, Adiabatic and nonadiabatic merging of independent Bose-Einstein condensates, *Phys. Rev. A* **71**, 043607 (2005).
- [25] R. Carretero-González, B. P. Anderson, P. G. Kevrekidis, D. J. Frantzeskakis, and C. N. Weiler, Dynamics of vortex formation in merging Bose-Einstein condensate fragments, *Phys. Rev. A* **77**, 033625 (2008).
- [26] L. Buchmann, G. Nikolopoulos, and P. Lambropoulos, Role of the relative phase in the merging of two indepen-

- dent Bose-Einstein condensates, *Phys. Rev. A* **79**, 013631 (2009).
- [27] R. G. Scott, A. M. Martin, T. M. Fromhold, and F. W. Sheard, Anomalous quantum reflection of Bose-Einstein condensates from a silicon surface: The role of dynamical excitations, *Phys. Rev. Lett.* **95**, 073201 (2005).
- [28] S. K. Adhikari, Self-trapping of a dipolar Bose-Einstein condensate in a double well, *Phys. Rev. A* **89**, 043609 (2014).
- [29] R. Roy, B. Chakrabarti, and A. Trombettoni, Quantum dynamics of few dipolar bosons in a double-well potential, *Eur. Phys. J. D* **76**, 24 (2022).
- [30] G. Spagnolli, G. Semeghini, L. Masi, G. Ferioli, A. Trenkwalder, S. Coop, M. Landini, L. Pezzè, G. Modugno, M. Inguscio, A. Smerzi, and M. Fattori, Crossing over from attractive to repulsive interactions in a tunneling bosonic Josephson junction, *Phys. Rev. Lett.* **118**, 230403 (2017).
- [31] G. Ferioli, G. Semeghini, L. Masi, G. Giusti, G. Modugno, M. Inguscio, A. Gallemí, A. Recati, and M. Fattori, Collisions of self-bound quantum droplets, *Phys. Rev. Lett.* **122**, 090401 (2019).
- [32] S. Gangwar, R. Ravisankar, P. Muruganandam, and P. K. Mishra, Dynamics of quantum solitons in lee-huang-yang spin-orbit-coupled bose-einstein condensates, *Phys. Rev. A* **106**, 063315 (2022).
- [33] T. Kanai, W. Guo, and M. Tsubota, Merging of rotating Bose-Einstein condensates, *J. Low Temp. Phys.* **195**, 37 (2019).
- [34] T. Kanai, W. Guo, M. Tsubota, and D. Jin, Torque and angular-momentum transfer in merging rotating Bose-Einstein condensates, *Phys. Rev. Lett.* **124**, 105302 (2020).
- [35] T. Kanai, W. Guo, and M. Tsubota, Flows with fractional quantum circulation in Bose-Einstein condensates induced by nontopological phase defects, *Phys. Rev. A* **97**, 013612 (2018).
- [36] R. Numasato and M. Tsubota, Numerical analysis of two-dimensional quantum turbulence, *J. Phys. Conf. Ser.* **150**, 032074 (2009).
- [37] R. Numasato and M. Tsubota, Possibility of inverse energy cascade in two-dimensional quantum turbulence, *J. Low Temp. Phys.* **158**, 415 (2009).
- [38] R. Numasato, M. Tsubota, and V. S. L'vov, Direct energy cascade in two-dimensional compressible quantum turbulence, *Phys. Rev. A* **81**, 063630 (2010).
- [39] S. Das, K. Mukherjee, and S. Majumder, Vortex formation and quantum turbulence with rotating paddle potentials in a two-dimensional binary Bose-Einstein condensate, *Phys. Rev. A* **106**, 023306 (2022).
- [40] J. A. Estrada, M. E. Brachet, and P. D. Mininni, Turbulence in rotating Bose-Einstein condensates, *Phys. Rev. A* **105**, 063321 (2022).
- [41] N. P. Müller, M.-E. Brachet, A. Alexakis, and P. D. Mininni, Abrupt transition between three-dimensional and two-dimensional quantum turbulence, *Phys. Rev. Lett.* **124**, 134501 (2020).
- [42] B. Marcelis, E. G. M. van Kempen, B. J. Verhaar, and S. J. J. M. F. Kokkelmans, Feshbach resonances with large background scattering length: Interplay with open-channel resonances, *Phys. Rev. A* **70**, 012701 (2004).
- [43] D. M. Bauer, M. Lettner, C. Vo, G. Rempe, and S. Dürr, Control of a magnetic feshbach resonance with laser light, *Nat. Phys.* **5**, 339 (2009).
- [44] C. Nore, M. Abid, and M. E. Brachet, Kolmogorov turbulence in low-temperature superflows, *Phys. Rev. Lett.* **78**, 3896 (1997).
- [45] A. S. Bradley, R. K. Kumar, S. Pal, and X. Yu, Spectral analysis for compressible quantum fluids, *Phys. Rev. A* **106**, 043322 (2022).
- [46] P. Muruganandam and S. K. Adhikari, Fortran programs for the time-dependent Gross-Pitaevskii equation in a fully anisotropic trap, *Comput. Phys. Commun.* **180**, 1888 (2009).
- [47] D. Vudragović, I. Vidanović, A. Balaž, P. Muruganandam, and S. K. Adhikari, C programs for solving the time-dependent Gross-Pitaevskii equation in a fully anisotropic trap, *Comput. Phys. Commun.* **183**, 2021 (2012).
- [48] L. E. Young-S, P. Muruganandam, S. K. Adhikari, V. Lončar, D. Vudragović, and A. Balaž, Openmp gnu and intel fortran programs for solving the time-dependent Gross-Pitaevskii equation, *Comput. Phys. Commun.* **220**, 503 (2017).
- [49] R. K. Kumar, V. Lončar, P. Muruganandam, S. K. Adhikari, and A. Balaž, C and fortran openmp programs for rotating Bose-Einstein condensates, *Comput. Phys. Commun.* **240**, 74 (2019).
- [50] A. Sivakumar, P. K. Mishra, A. A. Hujeirat, and P. Muruganandam, Energy spectra and fluxes of turbulent rotating Bose-Einstein condensates in two dimensions (2023), [arXiv:2310.06741](https://arxiv.org/abs/2310.06741) [cond-mat.quant-gas].
- [51] G. Verma, U. D. Rapol, and R. Nath, Generation of dark solitons and their instability dynamics in two-dimensional condensates, *Phys. Rev. A* **95**, 043618 (2017).
- [52] G. Theocharis, D. J. Frantzeskakis, P. G. Kevrekidis, B. A. Malomed, and Y. S. Kivshar, Ring dark solitons and vortex necklaces in Bose-Einstein condensates, *Phys. Rev. Lett.* **90**, 120403 (2003).
- [53] A. V. Mamaev, M. Saffman, and A. A. Zozulya, Propagation of dark stripe beams in nonlinear media: Snake instability and creation of optical vortices, *Phys. Rev. Lett.* **76**, 2262 (1996).
- [54] L. A. Smirnov and A. I. Smirnov, Scattering of two-dimensional dark solitons by a single quantum vortex in a Bose-Einstein condensate, *Phys. Rev. A* **92**, 013636 (2015).
- [55] A. J. Groszek, T. P. Simula, D. M. Paganin, and K. Helmersson, Onsager vortex formation in Bose-Einstein condensates in two-dimensional power-law traps, *Phys. Rev. A* **93**, 043614 (2016).
- [56] Á. V. M. Marino, L. Madeira, A. Cidrim, F. E. A. dos Santos, and V. S. Bagnato, Momentum distribution of vinen turbulence in trapped atomic Bose-Einstein condensates, *Eur. Phys. J.: Spec. Top.* **230**, 809 (2021).
- [57] A. Cidrim, A. C. White, A. J. Allen, V. S. Bagnato, and C. F. Barenghi, Vinen turbulence via the decay of multicharged vortices in trapped atomic Bose-Einstein condensates, *Phys. Rev. A* **96**, 023617 (2017).
- [58] C. Barenghi, H. Middleton-Spencer, L. Galantucci, and N. Parker, Types of quantum turbulence, *AVS Quantum Sci.* **5**, 025601 (2023).